*IOSR Journal of Applied Geology and Geophysics (IOSR-JAGG)*
*e-ISSN: 2321–0990, p-ISSN: 2321–0982.Volume 11, Issue 1 Ser. I (Jan. – Feb. 2023), 50-64*
*www.iosrjournals.org*

# Analysisand Interpretation of 3DMagnetotelluric Data to Delineate Geothermal Structures in Olkaria South East Field

Eunice. W. Wachira, Maurice O. k'Orowe, Justus Maithya, Anna Mwangi

***ABSTRACT***
*The Magnetotellurics(MT) method was used to characterize anddelineate the extent of the geothermal resource in Olkaria South East geothermal field, Kenya. The static shift effects of the MT datasets were corrected using the spatial median filter method.*

*Dimensionality analyses performed using phase tensor showed lower skews at short periods and higher skews at long periods, indicating 1D and 2D characteristics at shallow depth and significant 3D structures at depth. 2D inversion was doneusing Occam to generate resistivity models of Olkaria South East field. 3D Inversion was also carried out using ModEM code due to its ability in mapping the deep-seated structures which are ambiguous giving inaccurate information when using 2D inversion. Both 2D and 3D results revealed presence of a relatively high resistivitylayer (10 – 40 ohm-m) at about 2.5 to 3km underlying a conductivelayer of resistivity < 5 ohm-m.*

Date of Submission: 10-02-2023 Date of Acceptance: 22-02-2023

## I. INTRODUCTION

Kenya is endowed with a huge geothermal resource due to the presence of the Kenya rift. Geothermal energy is a clean and renewable source of energy, which is not affected by short-term fluctuations in the weather. Once installed, maintenance costs are low and availability high as evident from the records of the Olkaria power stations in Kenya (Lagat*et al*., 2007; Kanda *et al*., 2011; Omenda and Simiyu, 2015). Olkaria Geothermal field is a high temperature geothermal resource in the Kenyan Rift Valley which has been used for electricity generation since 1981 (Figure 1).

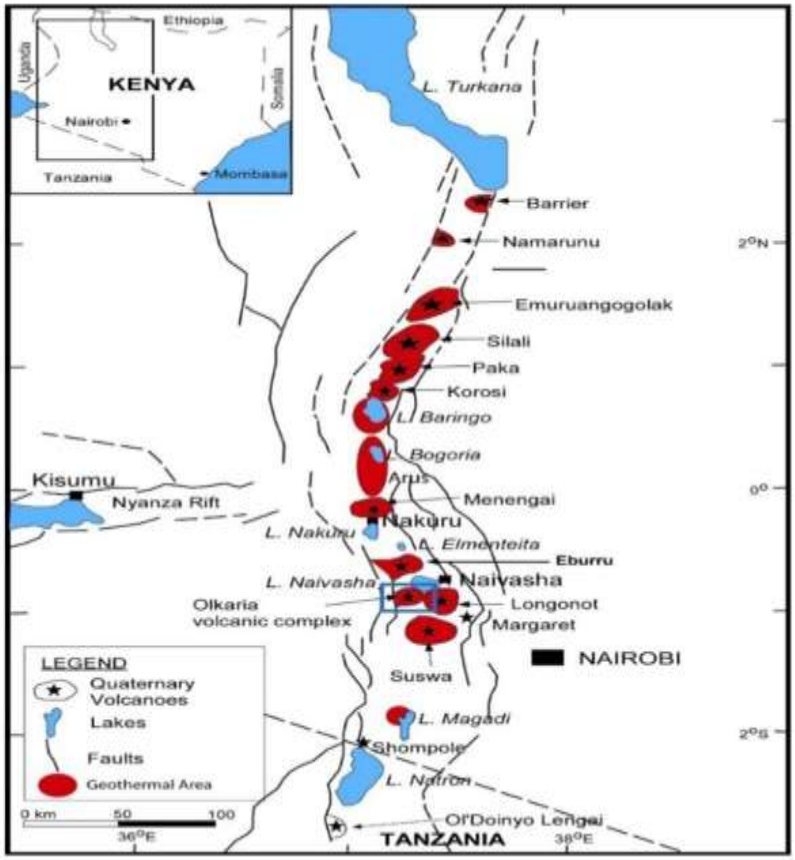


**Figure 1:** Map of Kenya showing the location of Olkaria geothermal field (Clarke *et al.,* 1990; Simiyu, 2010).

Olkaria geothermal field is subdivided into seven sectors for geothermal development purposes namely: Olkaria East, Olkaria Northeast, Olkaria Central, Olkaria Northwest, Olkaria Southwest, Olkaria Southeast and Olkaria Domes (Figure 2). The Olkaria South East field is still in the early stages of exploitation with at least 20 geothermal wells drilled (Ngetich, 2016).

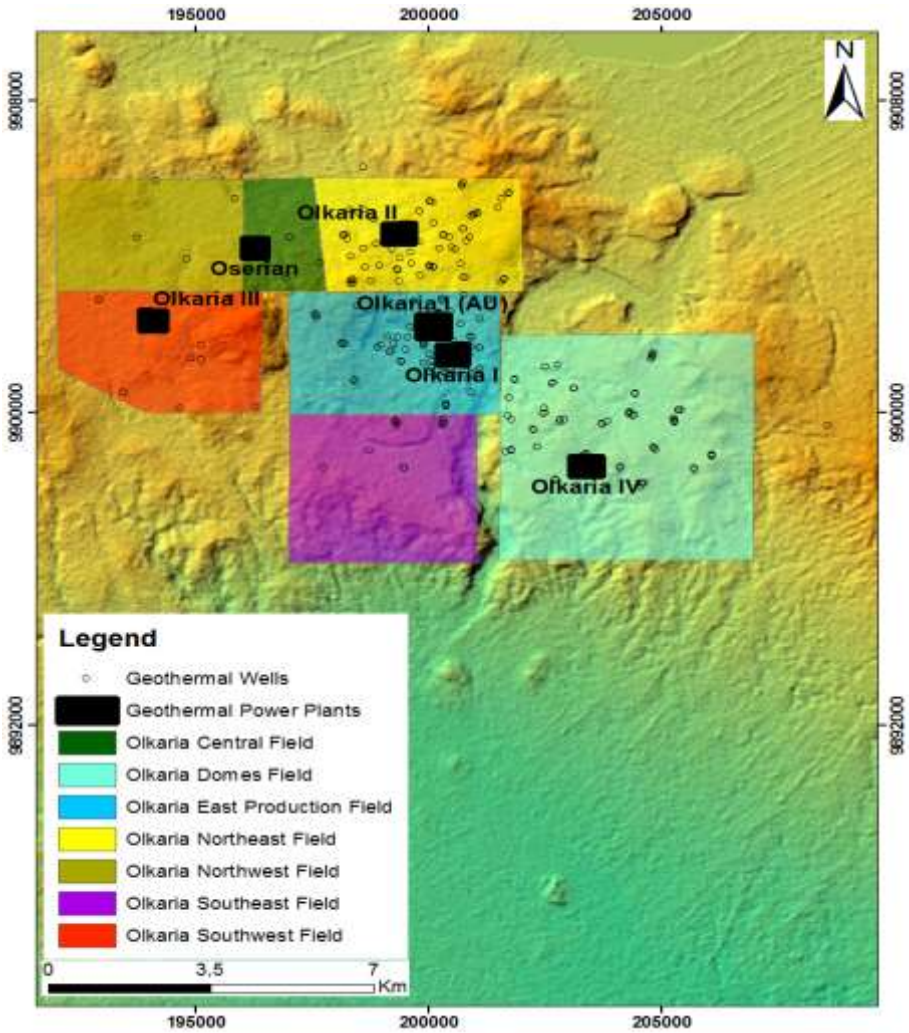


**Figure 2:** Sub-sectors of the Greater Olkaria Geothermal Field. License by December, 2015 (Munyiri, 2016).

Geophysics techniques have been used in the investigation of geothermal prospects since they give detailed information of the subsurface without drilling (Telford *et al*., 1990; Parasnis, 1997). Zones of low resistivity associated with geothermal reservoirs can be detected by geophysical techniques such as the magnetotellurics (MT) method which is now widely applied to natural resources exploration. Higher temperatures, salinity of the pore water and naturally accompanying increased rock alteration associated with geothermal areas often contribute to this decrease in the bulk resistivity in a rock mass.

The MT method utilizes natural variations in the Earth's magnetic field as a source. The fluctuations in the natural magnetic field of the earth **B** and the induced electric field **E** are measured. The electrical properties such as electrical conductivity of the underlying material can be determined from the relationship between the components of the measured electric (E) and magnetic field (B) variations, or transfer functions which arethe horizontal electric (Ex and Ey) and horizontal (Bx and By) and vertical (Bz) magnetic field components (Naidu, 2012).The basic MT response, Z also known as the impedance tensor, can be defined as the linear relationship between horizontal electric and magnetic field variations at a specific station at the Earth's surface. Z, is frequency dependent and contains the information about the subsurface conductivity structures.

Natural MT signals come from a variety of natural currents including thunderstorms and solar winds. Due to the large frequency spectrum of the geomagnetic field MT, can investigate the earth from tens of meters to tens of kilometers which makes the method suitable for exploration of basins as well as mature fields. It has a good resolution and applicable in difficult environments since it's an induction technique. The total frequency range of MT data spans 40 kHz to less than 0.1 mHz. MT data is used to investigate the shallow to deep subsurface geo-electrical structures and their dimensions. In order to have a higher accuracy in modeling the MT data, dimensionality analysis of the subsurface structures should be determined (Filbandi, 2016).

2D inversion has been the standard technique for MT data interpretation in the past decade. It has provided detailed resistivity models in many geothermal fields contributing to the understanding of the resistivity features of a geothermal reservoir. However, 2D interpretations sometimes has limitations and fails to

produce realistic models due to the complicated geological environments in the geothermal fields (Uchida and Sasaki, 2006).

## II. Geological setting of the Study Area

The Greater Olkaria Volcanic Complex (GOVC), is characterized by comendite lava flows and pyroclastics on the surface and basalts, trachytes and tuffs in the subsurface (Figure 3) (Marshall*et al*., 2008). Olkaria wells have plateau trachytes occurring from depth of approximately 1000m to 3000m. These trachytes often appear in conjunction with minor basalts, tuffs and rhyolites. The Olkaria basalts underlie the upper Olkaria volcanics east to the Olkaria Hill and consist of basalts with minor pyroclastics and trachytes to the west of the Olkaria Hill (Omenda, 2000).

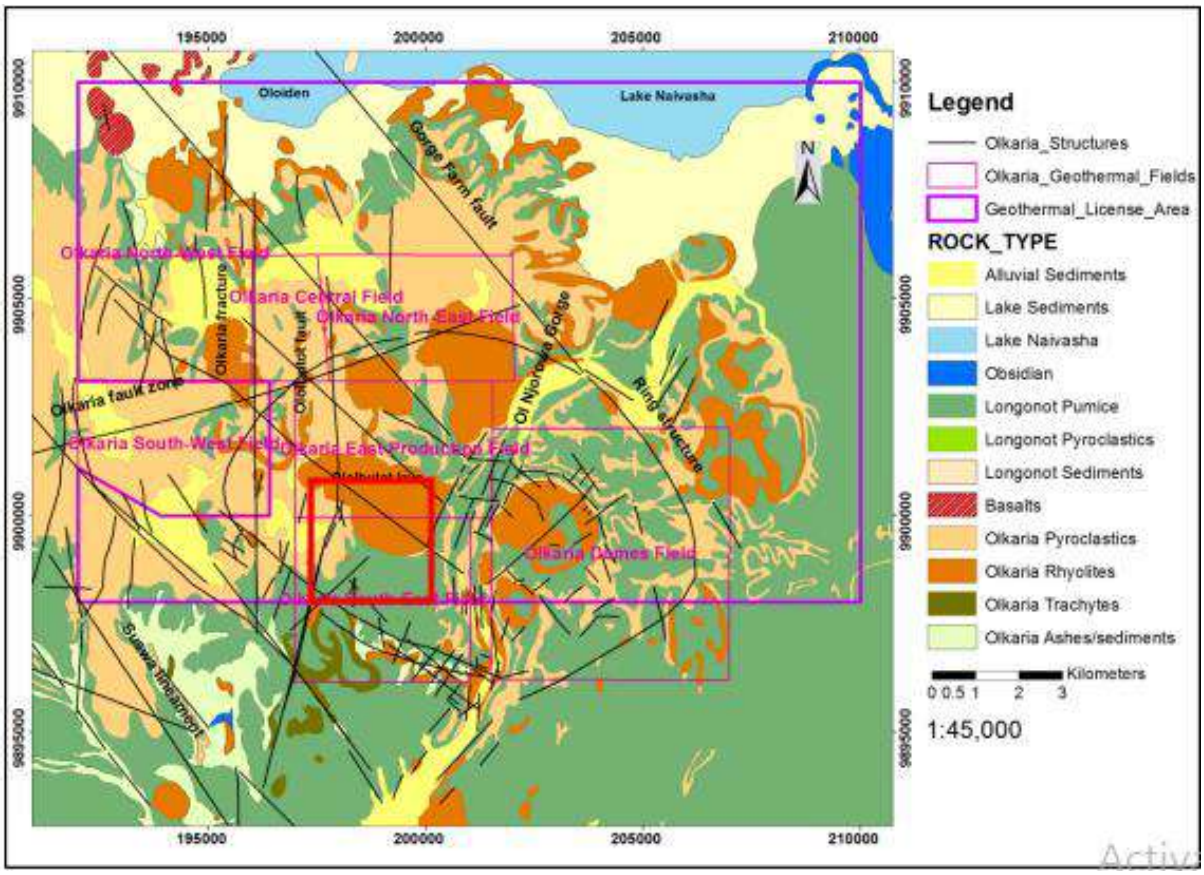


**Figure 3**: The geology of the Greater Olkaria Volcanic Complex (Marshall *et al*., 2008).

## III. Previous geophysical studies

In Olkaria, direct current resistivity methods have been used for reconnaissance mapping, location of faults for drilling targets and to define the boundaries of geothermal reservoirs (Wamalwa *et al*., 2013). MT and TEM are the commonest resistivity methods applied during prospecting for geothermal energy. These methods are used to measure electrical resistivity with depth. Low resistivities are generally associated with geothermal reservoirs and are due to the presence of hot rocks and saline hot waters (Wanjohi, 2014).

Resistivity data interpretation from the Olkaria geothermal field shows that the low resistivity (less than 20 Ωm) anomalies at depths of 1000 ma.s.l that define the geothermal resource boundaries are controlled by linear structures in the NE-SW and NW-SE directions (Mulwa and Mariita, 2013, 2015; Wamalwa and Serpa, 2013; Abdelfettah*et al*., 2016). Drilled wells show that the low resistivity anomalies at 1000 m.a.s.l define a geothermal system with temperatures in excess of 240 $^0$C (Ofwona, 2008). Some of the high resistivity regions coincide with recharge areas associated with NE and NW trending faults that act as conduits for cold water flow from the Rift Valley scarps. The geothermal fluid up-flow zones occur at the intersections of these regional faults in the vicinity of a heat source.

Dimensionality analysis performed in Olkaria geothermal field showed the data is 3D and this is supported by the 3D nature of the underlying major structures (Mwangi *et al*., 2008).

MT data for the Aluto-Langano geothermal field were evaluated and inverted in 3D using ModEM program. The recovered 3D resistivity model revealed structures that corresponds very well to the conceptual model for high-enthalpy volcanic geothermal systems (Abera*et al*., 2018).

3D MT inversion was also conducted in Kakkonda geothermal field located in Iwate prefecture, Japan. GRRI-3D algorithm was applied to these MT data and a resistivity structure of Kakkonda geothermal field was recovered (Yamane *et al*., 1998).As of 2000, 3D inversions of MT data have been used for geothermal exploration (Yamane *et al*., 2000).

In Iceland, (Gasperikova*et al*., 2011) successfully imaged Krafla and Hengill geothermal reservoir fields using 3D MT inversions.

Because the Earth is 3D, a 2D Earth model cannot be used to explain or represent the 3D Earth and it will be based on assumptions. If the data contains 3D structures, 2D inversion can mislead an interpretation. In this study 2D and 3D magnetotellurics data inversion were carried out to characterize the geothermal resource in Olkaria South East field.

## IV. Magnetotellurics Method

Natural electromagnetic (EM) signals are generated from two sources which are: At the lower frequencies, generally less than 1 Hz, or more than 1 cycle per second, and the high frequency signal greater than 1 Hz or less than 1 cycle per second. The lower frequency signal originates from the interaction of the solar wind with the earth's magnetic field while the high frequency signal is created by world-wide thunderstorm activity, usually near the equator. The above signal sources create a measurable time varying electromagnetic wave (Tikhonov, 1950; Cagniard, 1953).

MT method is a passive electromagnetic method which uses electric and magnetic field variations of natural origin (Vozoff, 1991). When this external energy, known as the primary electromagnetic field, reaches the earth's surface, part of it is reflected back and remaining part penetrates into the earth. Earth acts as a good conductor, thus electric currents (known as telluric currents) are induced in turn to produce a secondary magnetic field.

The relation between electric and magnetic fields as a function of period (or frequency) determines the subsurface electrical conductivity distribution (Tikhonov, 1950; Cagniard, 1953).

The apparent resistivity, $\boldsymbol{\rho_a}$ is derived from the ratio of electric and magnetic magnitudes given by:

$$\boldsymbol{\rho_a} = \frac{\mathbf{0.2}}{\boldsymbol{f}}\left|\frac{\boldsymbol{E}}{\boldsymbol{B}}\right|^{\mathbf{2}} \tag{1}$$

where **f** is the frequency, **E** is the electric field and **B** is the magnetic field.

As electromagnetic fields diffuse into a medium, they decay exponentially, the principle of skin depth which is given by:

$$\boldsymbol{d(T)} = \sqrt{\frac{\boldsymbol{T}}{\boldsymbol{\pi\mu\sigma}}} \tag{2}$$

where $\boldsymbol{d(T)}$ is the electromagnetic skin depth in meters at a given period **T**, **σ** is the conductivity of the medium penetrated and **μ** is the magnetic permeability. The electromagnetic fields are attenuated to $e^{-1}$ of their amplitudes at the surface of the earth, at a depth $d(T)$. This exponential decay of electromagnetic field with increasing depth renders them insensitive to deeper lying conductivity structure than $d(T)$.

Therefore, in MT, one electromagnetic skin depth is generally equated to the penetrating depth of the electromagnetic fields into the earth given by:

$$d(T) = 503\sqrt{Tp_a} \tag{3}$$

where $\boldsymbol{\rho_a}$is the apparent resistivity of an equivalent uniform half space (Simpson & Bahr, 2005). Therefore, at a zeroth order conceptual level, magnetotellurics comprises measurements of the skin depth as a function of period to infer resistivity as a function of position in earth.

**Magnetotelluric Transfer Functions**

MT transfer functions or MT responses are functions that relate the registered electromagnetic field components at given frequencies. MT responses only depend on the electrical properties of the material and not the electromagnetic source. Therefore, they characterize the conductivity distribution of the underlying materials according to the measured frequency. They include:

***Impedance Tensor***

The relation between electric and magnetic field is described by the following equation which can be represented in a matrix form as:

$$\begin{bmatrix} \boldsymbol{E_x} \\ \boldsymbol{E_y} \end{bmatrix} = \begin{bmatrix} \boldsymbol{Z_{xx}} & \boldsymbol{Z_{xy}} \\ \boldsymbol{Z_{yx}} & \boldsymbol{Z_{yy}} \end{bmatrix} \begin{bmatrix} \boldsymbol{H_x} \\ \boldsymbol{H_y} \end{bmatrix} \quad (4)$$

The impedance **Z** is a complex tensor and is a function of the earth's resistivity $\rho$.The asymmetry of the material is given by on-diagonal components of Z. They become zero if the material is symmetric about a vertical plane passing through the observation site (Berdichevsky and Dmitriev, 2002). The off-diagonal components of Z give the information about vertical variations in resistivity structure. The spatial distribution of resistivity can be classified in three ways:

In case of a 1D earth, the resistivity changes with depth only. The impedance tensor can be written as:

$$\boldsymbol{Z} = \begin{bmatrix} \boldsymbol{0} & \boldsymbol{Z_{xy}} \\ \boldsymbol{Z_{yx}} & \boldsymbol{0} \end{bmatrix} \quad (5)$$

where $Z_{xy} = -Z_{yx} \neq 0$

In a 2D earth, resistivity varies with depth and in one horizontal direction. The direction in which resistivity remains constant is called geoelectric strike. The impedance tensor is given by:

$$\boldsymbol{Z} = \begin{bmatrix} \boldsymbol{0} & \boldsymbol{Z_{xy}} \\ \boldsymbol{Z_{yx}} & \boldsymbol{0} \end{bmatrix} \quad (6)$$

But $Z_{xy} \neq Z_{yx}$

In 3D earth, resistivity varies in all the three directions and the impedance tensor is given by:

$$\boldsymbol{Z} = \begin{bmatrix} \boldsymbol{Z_{xx}} & \boldsymbol{Z_{xy}} \\ \boldsymbol{Z_{yx}} & \boldsymbol{Z_{yy}} \end{bmatrix} \quad (7)$$

$Z_{xx} \neq Z_{yy}$ & $Z_{xy} \neq Z_{yx}$

***Geomagnetic Transfer Functions***

Geomagnetic transfer functions **T** also known as tipper vector is a dimensionless complex vectoral magnitude. $\vec{T} = R_e(\vec{T}) + i.Im(\vec{T})$ and is defined as the relation between the vertical and the two horixontal components of the magntic field.

$$\boldsymbol{B_z} = (\boldsymbol{T_x}, \boldsymbol{T_y}).\begin{pmatrix} \boldsymbol{B_x} \\ \boldsymbol{B_y} \end{pmatrix} \quad (8)$$

The tipper vector can be decomposed into two real vectors in the xy plane, corresponding to its real and imaginary parts. The real vectors are also called induction vectors or induction arrows and they are used to infer the presence of lateral variations in conductivity.

**1.4MT survey and data acquisition**

The MT data was collected by KenGen between 2010 and 2021using the Phoenix MTU -5 instruments.The MT unit consists of a data logger, global positioning system (GPS), three magnetic coils (Hx, Hy, and Hz), 12V battery and five non-polarizing electrodes. The distance between eachpair of electrodes (Ex and Ey) was 60m. To ensure good conductivity the electrodes were soaked in a sodium chloride solution. The three magnetic coils were buried at a depth of one foot and oriented as shown in the Figure 4. The four telluric ports were also buried shallowly with a solution of bentonite. The car battery was used to power the system. Data was collected at the station identified by the GPS and data was collected continuously for at least 18 hours at each station. A total of 23 MT stations were used for this study.

Time series data was downloaded from the MT unit using SSMT2000 program and then processed to transform them into frequency domain expression in terms of apparent resistivities and phase of impedance as a function of frequency for each station. The time series data was Fourier transformed then processed and edited in the MT Editor program provided by phoenix Geophysics- Canada.

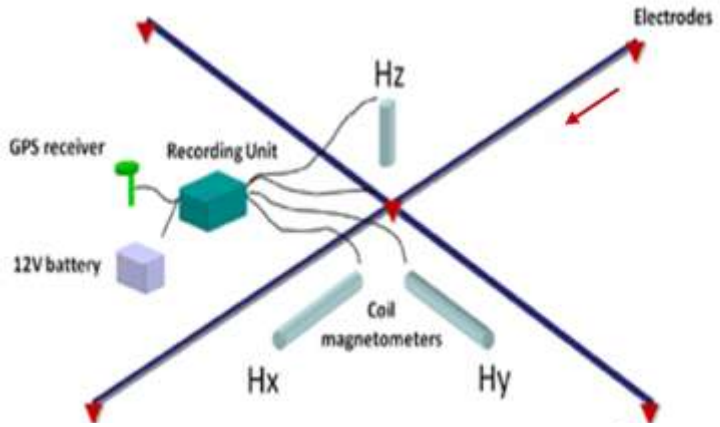


Figure 4: Typical Field MT setup

## V. DATA ANALYSIS

### 5.1 Dimensionality Analysis

Dimensionality analysis of MT data is a common procedure for inferring the main properties of the subsurface geo-electric structures such as the strike direction or the presence of superficial distorting bodies, and helps in determining the most appropriate modeling approach (Martí *et al*., 2010).

### 5.2 Phase tensor analysis

Phase tensor provides better solution for dimensionality and strike direction and is not affected by galvanic distortion. The phase tensor **Φ** is defined as the ratio of the real (***X***) and imaginary parts (***Y***) of the complex impedance tensor, **Z**.

$$\Phi = Y/X \tag{9}$$

where

$$Z = X + iY \tag{10}$$

The phase tensor can beillustrated graphically (Figure 5) by an ellipse consisting of skew angle (β) and minimum ($\Phi_{min}$) and maximum ($\Phi_{max}$) principal axes. In phase tensor maps, the skew angle value is mostly displayed as colour filling of the ellipses. The phase tensor can be expressed in terms of$\alpha$, β, $\Phi_{min}$and $\Phi_{max}$as shown in equation 11:

$$\Phi = RT(\alpha - \beta)\begin{bmatrix}\Phi max & 0\\ 0 & \Phi min\end{bmatrix}R(\alpha + \beta) \tag{11}$$

where ***R*** ($\alpha$+ β) is the rotation matrix and ***RT*** is inverse rotation matrix. The strike of the major axis of the ellipse is given by α − β, and in the case of a 2D or 3D/2D Earth, $\beta$ is zero and the 2-D strike direction is given by α.

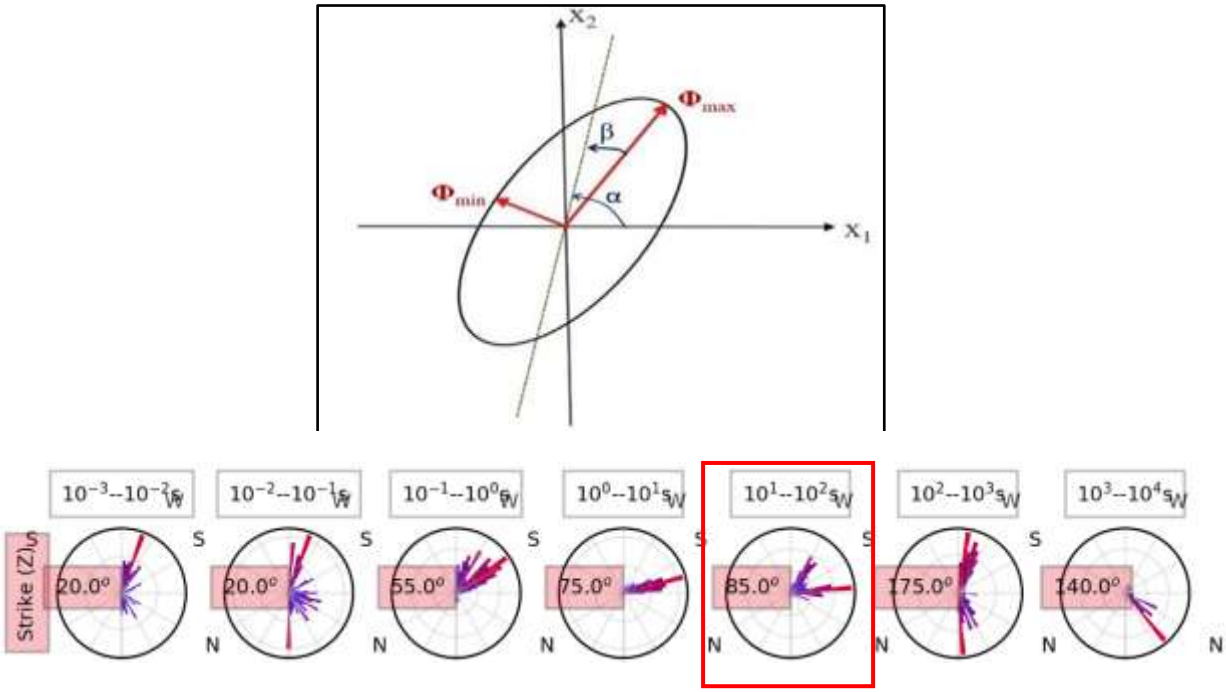


**Figure 5 a**: Graphical representation of phase tensor (Caldwell *et al*., 2004). The skew angle, β is needed as a third coordinate invariant if the phase tensor is non-symmetrical to characterize the tensor. The angle α - β, which gives the orientation of the major axis of the ellipse, defines the relationship between the tensor and the observational reference frame (x1 and x2) **(b)** Geo-electric strike rose diagramsof S75$^{O}$W at periods $10^{0}$ – $10^{1}$ s, which conforms to the Olkaria field regional structural trend of NE-SW. The profiles 1 and 2 were constructed nearly parallel and perpendicular to the geo-electric strike direction respectively.

For 1D case, the phase tensor is characterized by a small skew angle and a circular shape. Naturally, if the conductivity is both isotropic and 1D, the radius of the circle will vary with period according to the variation of the conductivity with depth. The radius will increase if the conductivity increases with depth. For a 2D regional resistivity structure, the phase tensor will be represented by an ellipse and β becomes zero for noise free data and close to zero for a field data. In the presence of 3D structure, the phase tensor is non-symmetric and a larger skew angle (β) value. Maps of the phase tensor ellipses at different periods provide a simple way of visualizing lateral changes in the regional conductivity structure at different depths. Such maps will not be influenced by near-surface galvanic effects (Caldwell *et al*., 2004).

In Olkaria south east, the phase tensor maps plotted at different frequencies reveal the dimensionality of the MT data (Figures 6 and 7). The shapes of the phase tensor and skew angle give an idea of the dimensionality of the subsurface structures. At high frequencies (short periods)the phase tensor maps indicate small skew angle ( $-3 < \beta < 3$) as observed in frequencies above 1 Hz. The shape of the ellipse generallyisyellow in color, circular at higher frequencies implying structures at shallow depths indicating 1-D and 2-D characteristics (Figure7). The phase tensor analysis reveals 3D dimensionality below1Hz, as deeper structures characterized by a high skew angle ($\beta < -3$ and $\beta > 3$), red, blue colors and the phase tensors are non-symmetric as indicated below 1 Hz, in Figure 7.


Figure6: Phase tensor map for 100Hz

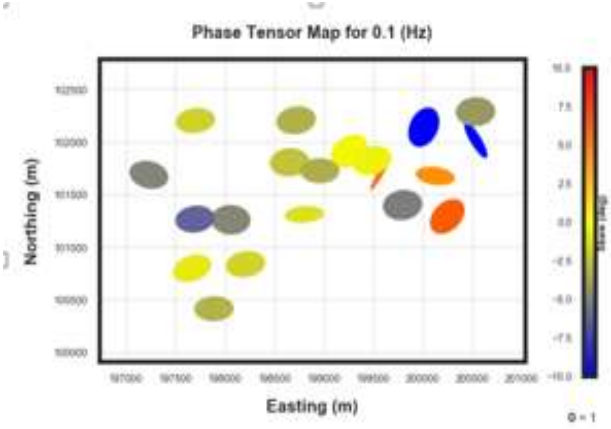


figure 7: Phase tensor map for 0.1Hz

### 5.3 Static Shift Correction

This is a constant displacement of the apparent resistivity along all frequencies caused by charge distribution accumulated on the surface of shallow bodies which produce an anomalous electromagnetic field. Static shift correction of the data was done using spatial median filter method. This method estimated the median of each polarization of the apparent resistivity for stations within a diameter of 2km and was compared to each station within the same radius for a given period range. If the difference is greater than a given tolerance, then that difference is assumed to be a static shift and is removed from the two components of the impedance for that polarization (Berdichesky& Dmitriev, 2008).

The ModEM program accounted for the remaining static shift effects by introducing a scattered conductivity distribution in the near-surface layers.

## VI. MT Data Inversion

### 6.1 2D inversion

2D inversion assumes that the resistivity varies with depth and in one lateral direction and that the resistivity is constant in the other horizontal direction (electrical strike). The coordinate axes are rotated until one of them is along strike.

Occam's 2D inversion code (version 3.0) developed by Scripps Institution of Oceanography based on deGroot-Hedlin and Constable (1990) was used for this study. Occam's 2D inversion is based on the minimization of the following unconstrained functional:

$$\boldsymbol{U = \|d_y m\|^2 + \|d_z m\|^2 + U^{-1}\left\{\|W(d - F(m))\|^2 - X^2,,\right\}} \qquad (12)$$

where the expression, $\boldsymbol{\|d_y m\|^2 + \|d_z m\|^2}$ is the norm of the model roughness, $\boldsymbol{U^{-1}}$ represents the Lagrange multiplier, the third term in the equation represents the data misfit, **W** is M x M diagonal weighting matrix, **d** represents the observation vector, and **F(m)** is the model response.For the 2D inversion a mesh with a block width set to 50m, 70 layers with an initial layer of 20m thickness increasing logarithmically with depth was generated for each profile. an initial model of 50 Ω*m*homogenous half-space was used. Maximum of 100 iterationsand a target root mean square of 0.5 was used with a maximum number of80 frequencies ranging from 0.011 Hz to 320 Hz. The models had a minimum root mean square misfit of 1.85 for profile 1 and 1.33 for profile 2.

### 6.2 Transverse electric (TE) mode and transverse magnetic (TM) mode

The 2D magnetotellurics field consists of two modes that is the TE and TM modes. The TM mode is related to the B-polarized wave generating the transverse MT curves (telluric current flows across the structures), and the TE mode is related to the E-polarized wave generating soundings MT curves (telluric current flows along the structures).

TM mode charges the structures and its anomalies galvanic in nature. TE on the other hand does not charge the structures and its anomalies are of inductive nature. The TM and TE modes offer different sensitivities to near-surface and deep structures and provide different accuracies of 2D approximation of real 3D bodies (Berdichevsky *et al.*, 1998).

For Profile 2 the pseudo-section plot for TE and TM modes for both observed and predicted in Fig.8shows a good fit. The TE mode shows a relatively better fit than the TM modes as it shows a small residual.

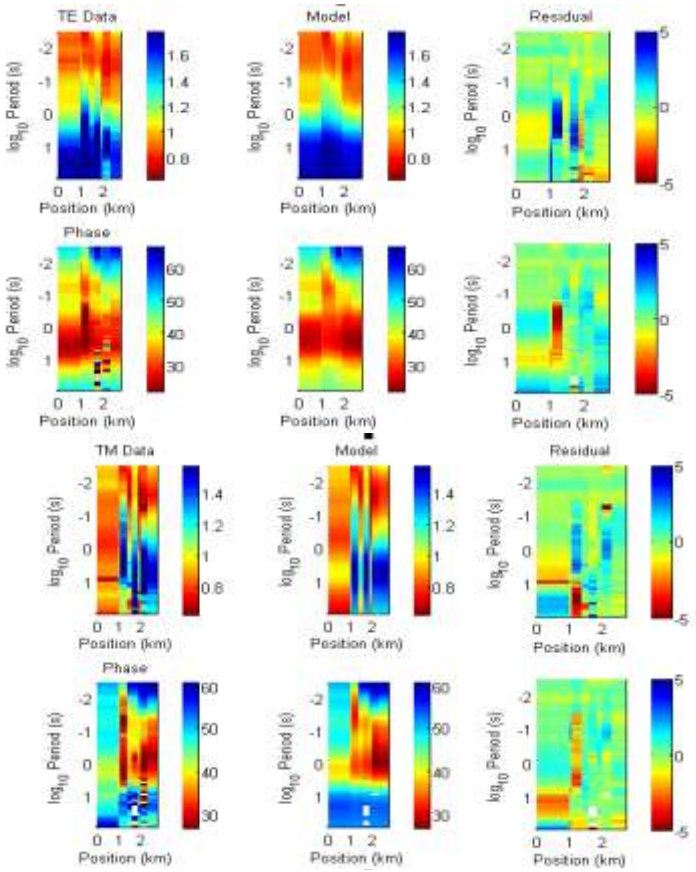


Fig 8: Pseudo sections of observed and calculated apparent resistivity and phase for TE and TM mode for Profile 2. The residual map shows the differences between the observed and predicted responses.

**4.0 2D Inversion results**

The resistivity models obtained from two profiles are as shown in figure 9 and 10.The results revealed conductive bodies C1 –C3 and resistive anomalies R1-R3. Figure 9 shows a conductive body C1 (< 10 Ωm) located at a depth of about 0.5 -3km and a resistive body R1 (> 100 Ωm) at a depth of 3-5km. figure 10 shows resistive bodies R2 and R3 separated by a conductive structure C2 running from NE to SW.C3 located at approximately 2-2.5km on the east side and separated from C2 by R3. It is also overlain by a conductive layer of approximately 0.5km and running deeper on the east side.

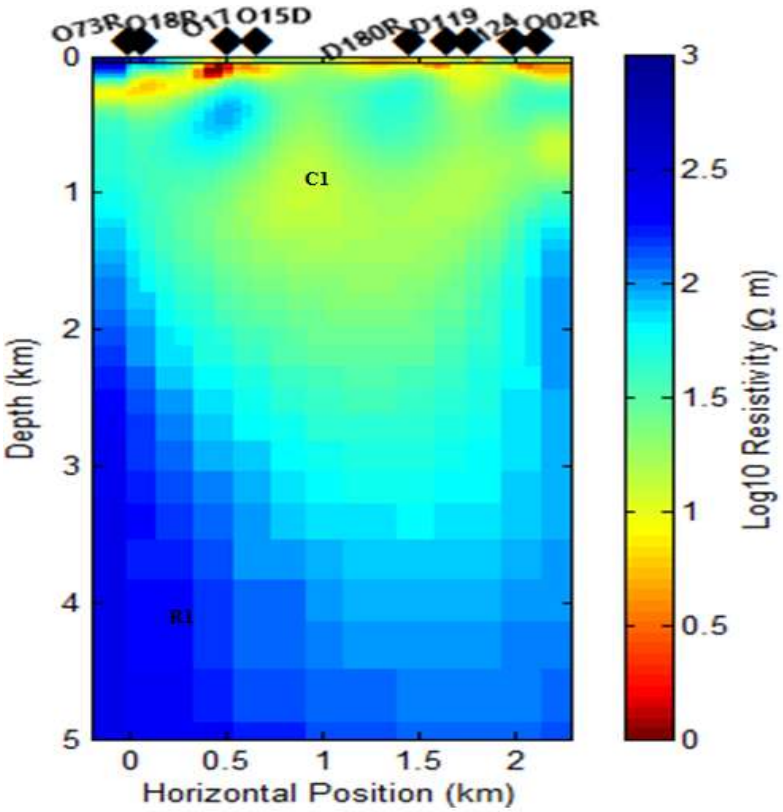


Figure 9: 2D resistivity cross-section model profile 1

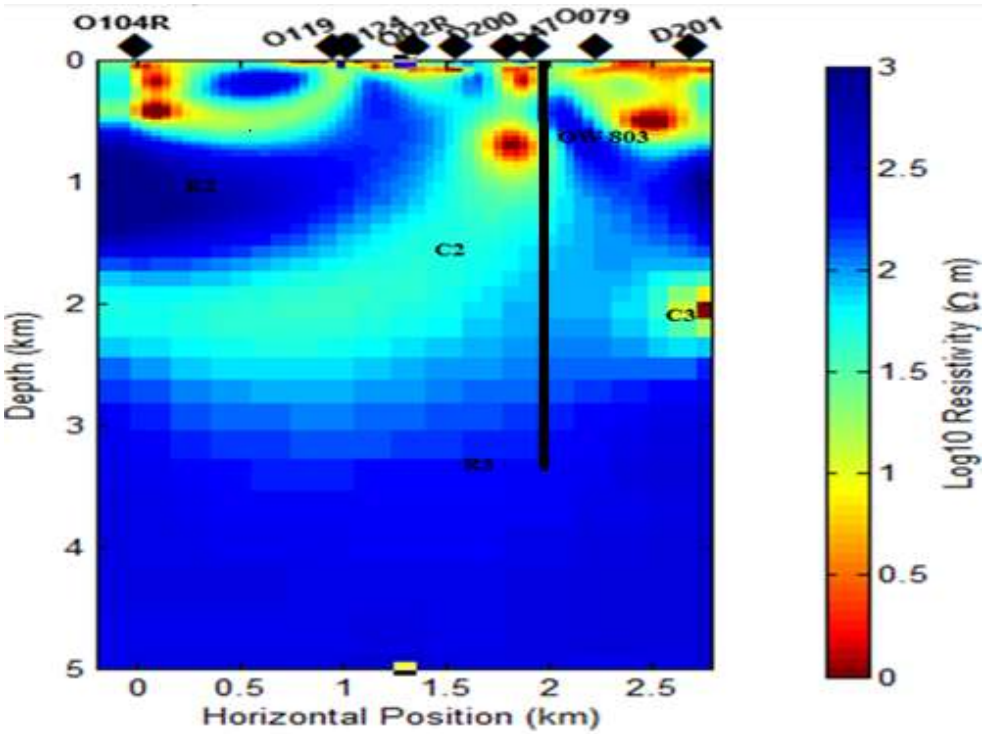


Figure 10: 2D resistivity cross-section model profile 2

### 6.3 3D Inversion

ModEM code developed by Egbert and Kelbert (2012), Meqbel (2009) and Kelbert et al. (2014) was used to analyze the MT data to produce a 3D resistivity models consistent with MT data that required it. The 3D inversion implemented in ModEM code is based on the minimization of the following penalty functional:

$$\boldsymbol{U(m,d) = \big(d - F(m)\big)^T C_d^{-1}\big(d - F(m)\big) + \lambda(m - m_0)^T C_m^{-1}(m - m_0)} \quad (13)$$

The first term in the equation represents the data misfit between the measured (**d**) and model response, **F**(**m**). The second term describes the model update between the estimated model (**m**) and initial model ($\mathbf{m_0}$). λ is the regularization parameter, $\mathbf{C}_m$ and $\mathbf{C}_d$ are the model and data covariance's, respectively. In ModEM the penalty function is minimized using the non-linear conjugate gradient (NLCG) method. The initial model, $\mathbf{m_0}$is updated iteratively by line search strategy. The 3D forward problem is based on the finite difference method (FDM).
A total of 23 MT stations were used for the 3D inversion. 50 layers were used with the first layer having a thickness of 10m and they increased with an increasing factor of 1.1. The resultant model is 5km deep with 38 * 50*50 cells in x,y and z directions respectively. ModEM achieved 93 iterations with a minimum root mean square misfit of5.48.

**3D results**

Two profiles same as the ones used in 2D inversion were used. The conductive (C1) and resistive R1 bodies in the 3D model had some similarities to those in the 2D model in profile 1. A resistive body C1 <10 ohm-m was observed at depth of about 1 to 2km on the east side. A high resistive layer > 10-45 ohm -m extended from 2.5km to around 3.5km likely to be the geothermal reservoir was obtained. Profile 2 showed two conductive layers C2 and C3 running from north east to south west separating resistive zones R2 and R3.

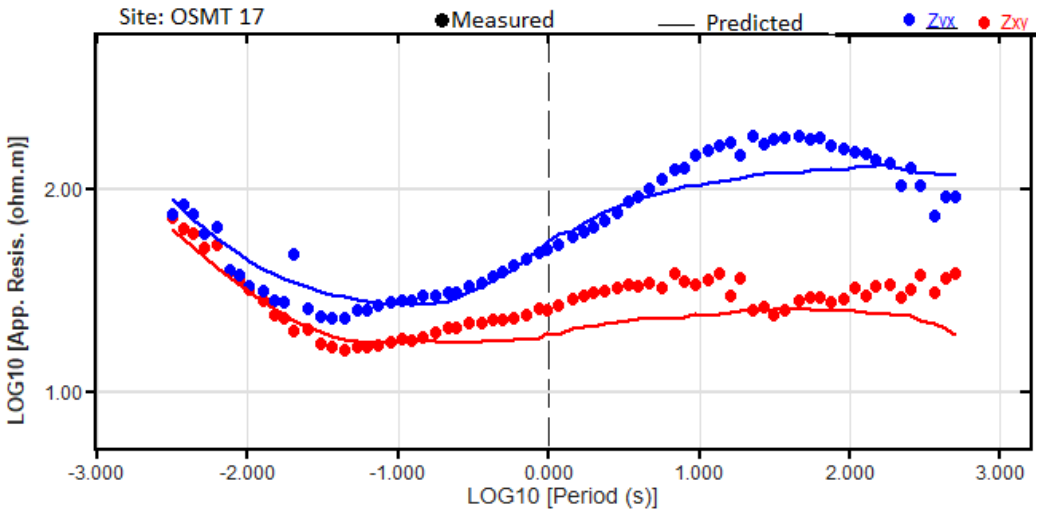


Figure 11: Data misfit between the observed and calculated apparent resistivity and phase parameters of Zxy (red dots) and Zyx (blue dots) components for station OSMT17. The dots represent themeasured values, and the line represents the calculated response.

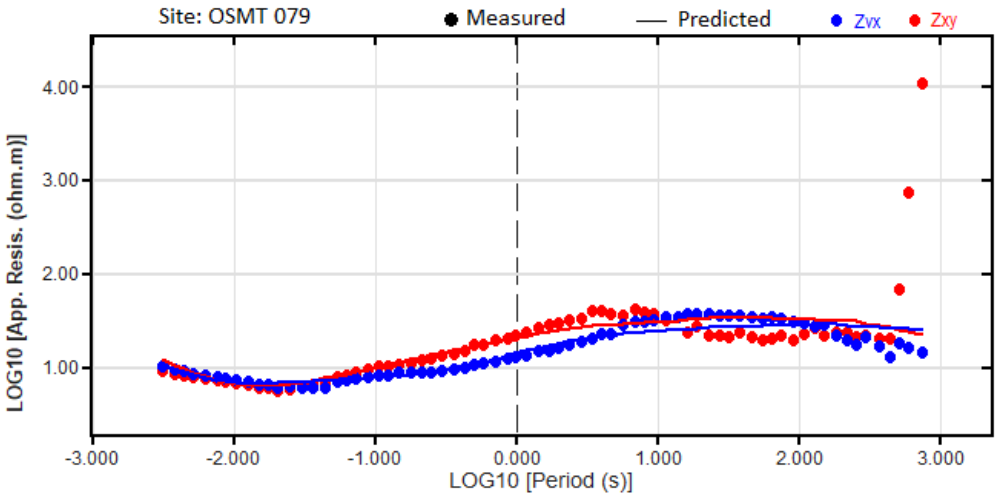


Figure 12: Data misfit between the observed and calculated apparent resistivity and phase parameters of Zxy (red dots) and Zyx (blue dots) components for station OSMT79. The dots represent themeasured values, and the line represents the calculated response.

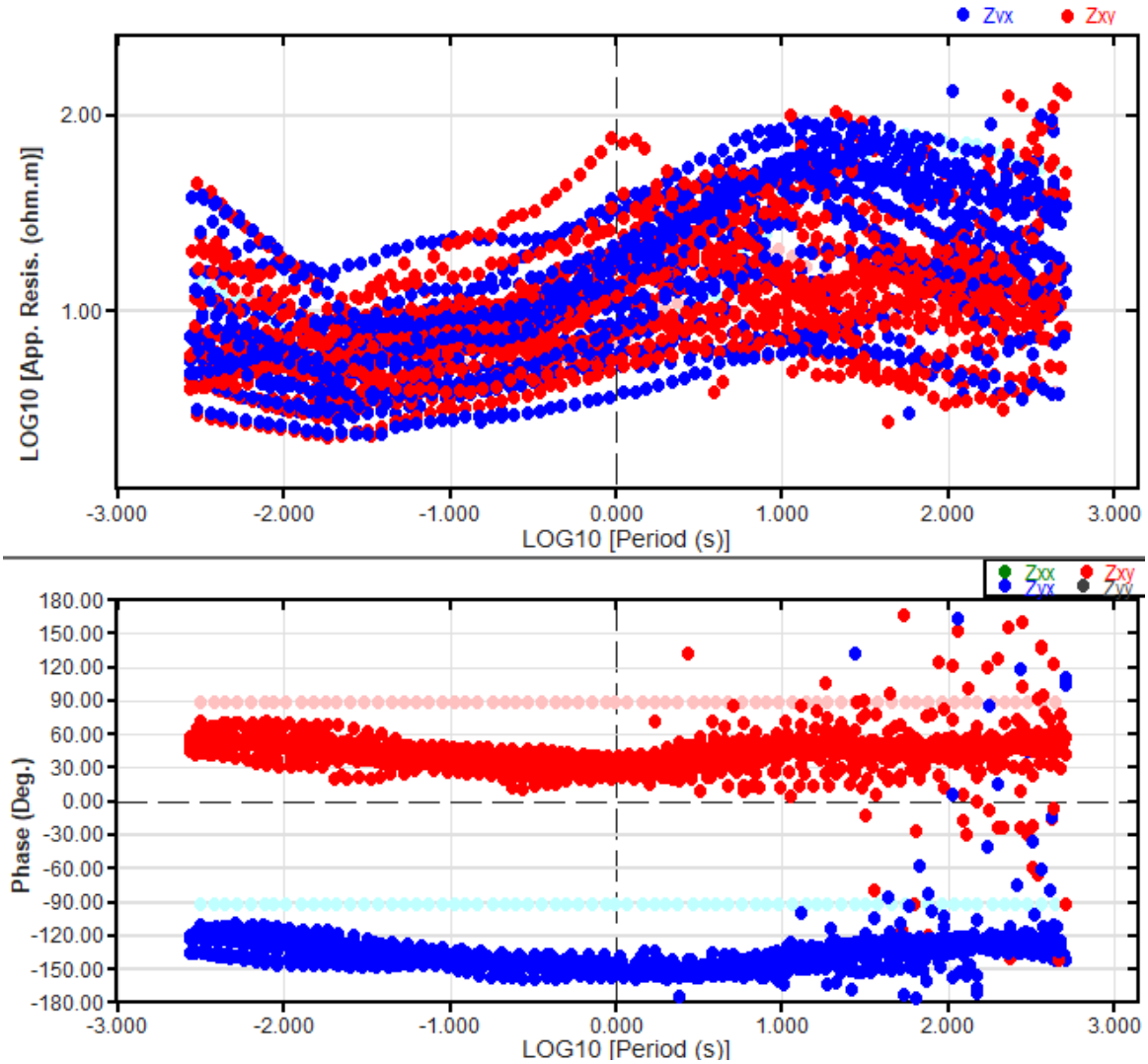


Figure 13: Apparent resistivity curves and phase curves from23 stations in Olkaria south east field respectively. The red dots indicate the TE mode and the blue dots indicate TMmode.

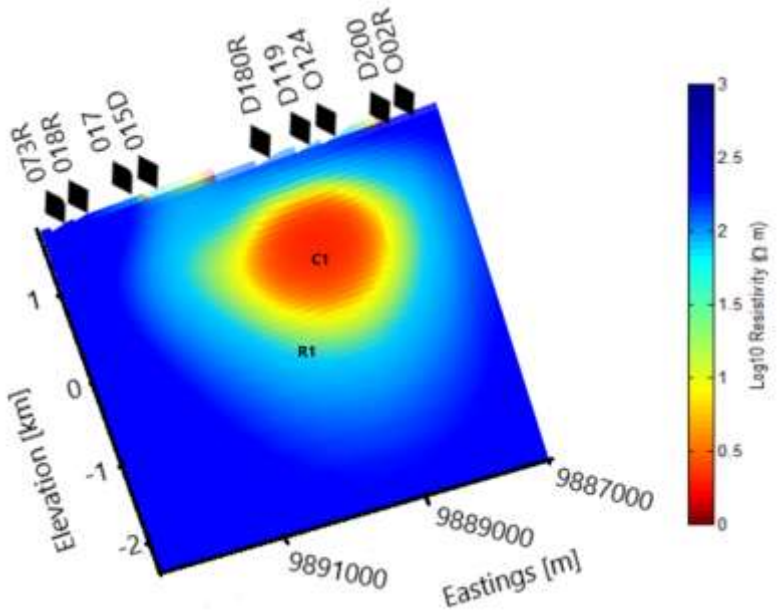


Figure 14: 3D resistivity model for profile 1.

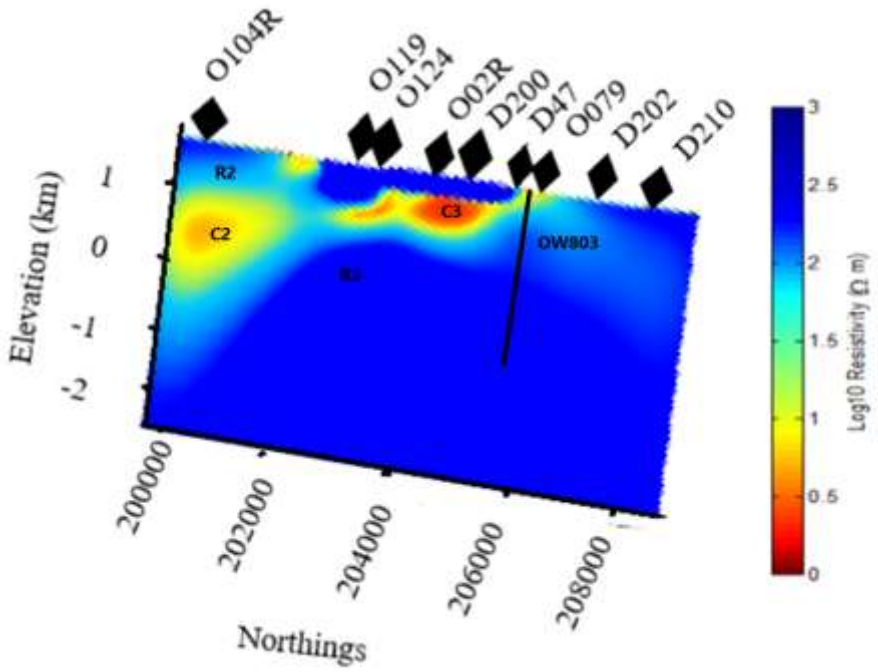


Figure 15: 3D resistivity model for profile 2

## VII. Discussion and Conclusion

Geological structures in Olkaria south east field trend in north-east to south-west and north-west to south-east direction. The profiles were cut perpendicular to the geological structures and horizontal models generated by 2D and 3D inversion. The results showed similar structures in the two profiles. Both 2D and 3D imaged same structures the same way but 3D imaged structures with a high resolution.

## REFERENCES

[1]. Abdelfettah, Y., Tiercelin, J. J., Tarits, P., Hautot, S., Maia, M., &Thuo, P. (2016). Subsurface structure and stratigraphy of the northwest end of the Turkana Basin, Northern Kenya Rift, as revealed by magnetotellurics and gravity joint inversion. Journal of African Earth Sciences, 119, 120-138.

[2]. Abera, C. B., Mizunaga, H., &Samrock, F. (2018). Imaging Resistivity Structures of High-Enthalpy Geothermal Systems Using Magnetotelluric Method: A case study of Aluto-Langano geothermal field in Ethiopia.

[3]. Berdichevsky, M. N., & Dmitriev, V. I. (2008). Models and methods of magnetotellurics. Springer Science & Business Media.

[4]. Berdichevsky, M. N., & Dmitriev, V. I. (2002). Magnetotellurics in the context of the theory of ill-posed problems. Society of Exploration Geophysicists.

[5]. Berdichevsky, M. N., Dmitriev, V. I., &Pozdnjakova, E. E. (1998). On two-dimensional interpretation of magnetotelluric soundings. Geophysical Journal International, 133(3), 585-606.

[6]. Caldwell, T. G., Bibby, H. M., & Brown, C. (2004). The magnetotelluric phase tensor. Geophysical Journal International, 158(2), 457-469.

[7]. Cagniard, L. (1953). Basic theory of the magneto-telluric method of geophysical prospecting. Geophysics, 18(3), 605-635.

[8]. Clarke, M. C. G., Woodhall, D. G., Allen, D., & Darling, G. (1990). Geology, volcanological and hydrogeological controls on the occurrence of geothermal activity in the area surrounding Lake Naivasha, Kenya. Report of the Ministry of Energy of Kenya.

[9]. deGroot-Hedlin, C., & Constable, S. (1990). Occam's inversion to generate smooth, two-dimensional models from magnetotelluric data. Geophysics, 55(12), 1613-1624.

[10]. Egbert, G. D., &Kelbert, A. (2012). Computational recipes for electromagnetic inverse problems. Geophysical Journal International, 189(1), 251-267.

[11]. Filbandi Kashkouli, M., Kamkar Rouhani, A., Moradzadeh, A., &Assi, H. (2016). Dimensionality analysis of subsurface structures in magnetotellurics using different methods (a case study: oil field in Southwest of Iran). Journal of Mining and Environment, 7(1), 119-126.

[12]. Gasperikova, E., Newman, G., Feucht, D., &Arnason, K. (2011). 3D MT characterization of two geothermal fields in Iceland. GRC Trans, 35(1-2), 1667-1671.

[13]. Kanda, I. K., Rankas, L., Bett, E. K., Kipngok, J. K., Mutonga, M., Sosi, B., ... &Mwawasi, H. (2011). Paka Prospect: Investigations of its geothermal potential (Vol. 10, p. 14pp). GDC Internal report.

[14]. Kelbert, A., Meqbel, N., Egbert, G. D., & Tandon, K. (2014). ModEM: A modular system for inversion of electromagnetic geophysical data. Computers & Geosciences, 66, 40-53.

[15]. Lagat, J. K., Omenda, P. O., Mungania, J., Mariita, N. O., Wambugu, J. M, Opondo, K. Ofwona, C., Mwawongo, G., Kubo, B. M., & Wetangula, G. (2007). Geo-scientific Evaluation of the Paka Geothermal Prospect, KenGen Internal report, 60,7pp.

[16]. Marshall, A., Macdonald, R., Rogers, N. W., Fitton, J. G., Tindle, A. G., Nejbert, K., & Hinton, R. W. (2008). Fractionation of peralkaline silicic magmas: The greater olkaria volcanic complex, Kenya Rift Valley. Journal of Petrology, 50(2), 323-359.

[17]. Martí, A., Queralt, P., Ledo, J., & Farquharson, C. (2010). Dimensionality imprint of electrical anisotropy in magnetotelluric responses. Physics of the Earth and Planetary Interiors, 182(3-4), 139-151.

[18]. Meqbel, N. M. M. (2009). The electrical conductivity structure of the Dead Sea Basin derived from 2D and 3D inversion of magnetotelluric data (Doctoral dissertation).

[19]. Mulwa, J., &Mariita, N. (2013). A comparative analysis of gravity and microseismic results from Arus-Bogoria geothermal prospect, Kenya. Scholarly Journal of Scientific Research and\Essay (SJSRE), ISSN, 2315-6163.

[20]. Mulwa, J. K., and Mariita, N. O. (2015). Dyking processes in Arus-Bogoria geothermal prospect in Kenya revealed using gravity and microseismic data. In 37th New Zealand Geothermal Workshop: The next 10,000 Megawatts. University of Auckland, New Zealand Geothermal Association, 37, 20-23.

[21]. Munyiri, S. K. (2016). Structural mapping of Olkaria Domes geothermal field using geochemical soil gas surveys, remote sensing and GIS (Doctoral dissertation).

[22]. Mwangi, A. W., Mickus, K., &Serpa, L. (2018). Dimensionality Analysis of the Olkaria Geothermal Field, East Africa Rift.

[23]. Naidu, G. D. (2012). Magnetotellurics: Basic theoretical concepts. In Deep Crustal Structure of the Son-Narmada-Tapti Lineament, Central India (pp. 13-35). Springer, Berlin, Heidelberg.

[24]. Ngetich, E. (2016). Characterization and Significance of Intrusive Rocks in Geothermal Reservoirs-Olkaria East and South East Fields. In Proceedings, 6th African Rift Geothermal Conference Addis Ababa, Ethiopia, 2nd–4th November.

[25]. Ofwona, C. (2008). Geothermal resource assessment–Case example, Olkaria I. Short Course III on Exploration for Geothermal Resources, UNU-GTP, 3, 18-19.

[26]. Omenda, P., & Simiyu, S. (2015). Country update report for Kenya 2010-2014. In Proceedings World Geothermal Congress (pp. 19-25).

[27]. Omenda, P. A. (2000). Anatectic origin for comendite in Olkaria geothermal field, Kenya rift: geochemical evidence for syenitic protolith. African Journal of Science and Technology, 1(2), 39-47.

[28]. Parasnis, D. S. (1997). Principles of Applied Geophysics: Chapman and Hall. London, England, 124-125.

[29]. Simiyu, S. M. (2010). Status of geothermal exploration in Kenya and future plans for its development. In Proceedings world geothermal congress (pp. 25-29).

[30]. Simpson, F., & Bahr, K. (2005). Practical magnetotellurics. Cambridge University Press.

[31]. Telford, W. M., Telford, W. M., Geldart, L. P., & Sheriff, R. E. (1990). Applied geophysics. Cambridge university press.

[32]. Tikhonov, A. N. (1950, February). On determining electrical characteristics of the deep layers of the Earth's crust. In Doklady (Vol. 73, No. 2, pp. 295-297). Citeseer.

[33]. Uchida, T., & Sasaki, Y. (2006). Stable 3D inversion of MT data and its application to geothermal exploration. Exploration Geophysics, 37(3), 223-230.

[34]. Vozoff, K. (1991). The magnetotelluric method. In Electromagnetic methods in applied geophysics: Volume 2, application, parts A and B (pp. 641-712). Society of exploration geophysicists.

[35]. Wamalwa, A. M., Mickus, K. L., &Serpa, L. F. (2013). Geophysical characterization of the Menengai volcano, Central Kenya Rift from the analysis of magnetotelluric and gravity data. Geophysics, 78(4), B187-B199.

[36]. Wamalwa, A. M., &Serpa, L. F. (2013). The investigation of the geothermal potential at the Silali volcano, Northern Kenya Rift, using electromagnetic data. Geothermics, 47, 89-96.

[37]. Wanjohi, A. W. (2014). Geophysical survey of a high-temperature field, Olkaria. Short Course IX on Exploration for Geothermal Resources, organized by UNU-GTP, GDC and KenGen, Kenya.

[38]. Yamane, K., Ohsato, K., Ohminato, T., & Kim, H. J. (2000). Three-dimensional magnetotelluric investigation in Kakkonda geothermal area, Japan. In proceedings world geothermal congress, Tohoku-Kyushu, Japan (pp. 1965-1968).

[39]. Yamane, K., Takasugi, S., Lee, K., &Ashida, Y. (1998). New magnetotelluric inversion scheme using generalized RRI method and case studies; GRRI ho niyoru MT o nijigen inversion kaiseki to sonotekiyorei. ButsuriTanko (Geophysical Exploration), 51.